Powder Technology 360 (2020) 96–103

Contents lists available at ScienceDirect

Powder Technology

journal homepage: www.elsevier.com/locate/powtec

High electrorheological effect in $Bi_{1.8}Fe_{1.2}SbO_7$ suspensions

A.V. Egorysheva [a,*], A.S. Kraev [b], O.M. Gajtko [a], T.V. Kusova [b], A.E. Baranchikov [a], A.V. Agafonov [b,c], V.K. Ivanov [a]

[a] Kurnakov Institute of General and Inorganic Chemistry, Russian Academy of Sciences, Moscow, 119991, Russia
[b] Krestov Institute of Solution Chemistry, Russian Academy of Sciences, Ivanovo, 153045, Russia
[c] National Research Tomsk State University, Tomsk, 634050, Russia

ARTICLE INFO

Article history:
Received 11 June 2019
Received in revised form 4 October 2019
Accepted 7 October 2019
Available online 13 October 2019

Keywords:
Nanoparticles
Pyrochlore
Complex bismuth oxides
Dielectric properties
Electrorheological effect
Electrorheological fluids

ABSTRACT

We report on the first experimental evidence of the electrorheological effect in suspensions of superfine pyrochlore-type $Bi_{1.8}Fe_{1.2}SbO_7$ powders. Tensile-compressive and shear stress studies of the electrorheological fluids, with various filler contents, revealed an exceptionally high electrorheological effect in the materials – the tensile yield strength at 5 kV/mm reached about 20 kPa. The frequency dependencies of dielectric permittivity, dielectric loss tangent, and the conductivity of the suspensions with various filler contents allowed estimation of the dielectric permittivity values for superfine $Bi_{1.8}Fe_{1.2}SbO_7$ particles at zero and infinite frequencies. The study reveals new oxide materials as promising fillers for electrorheological fluids.

1. Introduction

Electrorheological fluids (ERFs) belong to a family of smart electroadaptive materials. The key property of ERFs is their ability to reversibly change (by several orders of magnitude) viscoplastic properties under an external electric field. ERFs attract a great deal of attention due to their numerous practical applications, including their use in electrocontrolled dampers, clutches, gripping devices and various electromechanical systems for robotics, space technology, biomechanics and biomedicine [1]. To create electrorheological fluids, submicron particles of dielectric materials (possessing high dielectric permittivity) are suspended in liquids with low dielectric permittivity. The electrorheological effect arises from the electrostatic interaction of the dispersed particles and changes in their spatial distribution upon the application of an electric field. Numerous theoretical and experimental studies of the electrorheological effect have been reported previously [2–10]. However, despite the vast interest in this class of materials, there are still no exact criteria for the choice for dispersed phase material which will ensure the high electrorheological response of an ERF. Up to now, the range of filler materials for ERFs has been rather limited and includes mainly silicon and titanium oxides, alkaline-earth metal titanates, aluminosilicates, carbon-based materials (for example, fullerenes) and certain semiconducting polymers [11–16].

Complex oxides with a pyrochlore structure usually possess high values of dielectric permittivity at room temperature and a low dielectric loss tangent in the MHz range. The best values have been achieved for $Bi_{1.5}ZnNb_{1.5}O_7$ (BZN) and $Bi_{1.5}MgNb_{1.5}O_7$ (ε = 70–200, tan $\delta = 10^{-4}$–10^{-3}) [17–19]. The excellent dielectric properties of these materials and relatively mild conditions for their synthesis (800–1000 °C) allow their practical application as microwave dielectric resonators, oscillators and filters. Very recently, variation in the dielectric properties of pyrochlores upon the application of electric and magnetic fields was found [20–22]. This effect opens up new areas for the use of these materials in multilayer ceramic capacitors, tunable filters, phase shifters, electrically redirecting antennas, *etc.*

The dielectric properties of complex bismuth oxides have been extensively studied for BZN solid solutions. Bismuth-containing pyrochlores possess abnormal temperature dependence of the dielectric constant at high temperatures (negative temperature coefficient), which is associated with the decrease in the conductivity of the material [23]. The strong relaxation of $Bi_{1.5}ZnNb_{1.5}O_7$ dielectric polarization was revealed by Liu et al. [17]. It is most likely to be caused by the presence of vacancies in cation and anion sublattices (Frenkel pairs), rather than structural disordering. The dielectric properties of such materials depend on their composition and structure [23–27]. It has been shown that the replacement of Nb with Ta or Sb results in a decrease in dielectric permittivity and an increase in the temperature coefficient [23]. Similar changes

* Corresponding author. Postal address: Kurnakov Institute of General and Inorganic Chemistry, Russian Academy of Sciences, Leninskii pr. 31, Moscow, 119991 Russia.
E-mail address: anna_egorysheva@rambler.ru (A.V. Egorysheva).

https://doi.org/10.1016/j.powtec.2019.10.027
0032-5910/

occur upon the addition of small amounts of vanadium(V) into $Bi_{1.5}ZnNb_{1.5-x}V_xO_7$ ($0.005 \le x \le 0.05$) ceramic materials [24]. In BZN, the replacement of zinc by iron results in a decrease in the dielectric permittivity value of the material [25]. In Bi_2FeNbO_7, dielectric permittivity ($\varepsilon = 120–100$), as well as dielectric loss tangent values, monotonically decrease upon an increase in electromagnetic frequency in the range of 40 Hz–1 MHz. However, the ε value at a frequency of 1 MHz remains sufficiently high to consider Bi_2FeNbO_7 as a potential material for microwave engineering. In $Bi_{2-x}Fe_{1.42+x}Te_{0.58}O_7$ solid solutions, dielectric permittivity increases with bismuth content growth [27].

In this study, we report on the first experimental evidence of the electrorheological activity of suspensions of superfine $Bi_{1.8}Fe_{1.2}SbO_7$ powders in dielectric media (silicone oil). For suspensions with various filler contents, we provided a detailed study of dielectric and mechanical properties – dielectric permittivity and dielectric loss tangent, conductivity at various frequencies, and the effect of the electric field strength on tensile-compressive and shear stresses.

2. Experimental details

Superfine $Bi_{1.8}Fe_{1.2}SbO_7$ powders were synthesized using the microwave-hydrothermal (MWHT) method, which is advantageous due to the uniformity of the reaction medium's heating, ensuring a high reaction rate and the phase and morphological homogeneity of the product. The synthesis of superfine powders of ternary oxides by soft chemical methods is usually a challenge in itself, due to the very different chemical properties of the components (*i.e.* different solubilities of the precursors in acids and alkalies). For the synthesis, we followed our previously reported approach [28]. As starting reagents for synthesis, we used high purity $Bi(NO_3)_3{\cdot}5H_2O$, $Fe(NO_3)_3\cdot 9H_2O$, Sb_2O_3, HNO_3 (conc. aq. solution) and NaOH. All chemicals were provided by Aldrich. To synthesize $Bi_{1.8}Fe_{1.2}SbO_7$, we dissolved iron and bismuth nitrates (1.5716 g of $Bi(NO_3)_3{\cdot}5H_2O$ and 0.8726 g of $Fe(NO_3)_3\cdot 9H_2O$) in nitric acid. Antimony oxide (0.2624 g of Sb_2O_3) was separately dissolved in an alkaline solution (5–8 M NaOH, 30 mL). The nitrate solution was added dropwise into the alkaline solution. The obtained suspension was magnetically stirred for 30 min, and then transferred into a 100 ml Teflon vessel and subjected to MWHT treatment in a Berghof Speedwave MWS-3+ setup operating at 2.45 GHz and with a power of 1450 W. The autoclaves were filled to 30% capacity. Teflon vessels were heated to 200 °C within 5 min. The duration of isothermal treatment was 30 min. After the synthesis, the product was centrifuged, thoroughly washed with distilled water and dried in air at 50°C overnight.

The phase composition of the samples was determined by powder X-ray diffraction (XRD) using a Bruker D8 Advance powder diffractometer with Ni filtered CuK_α radiation and a LYNXEYE detector. The diffraction data were collected in the 2θ range from 3° to 100°, in steps of 0.02° and a collection time of 0.4 s/step. The Rietveld refinement was performed using the TOPAS 4.2 software (Bruker AXS, Karlsruhe, Germany). The morphology of the samples was examined using a Carl Zeiss NVision 40 scanning electron microscope (SEM) at an accelerating voltage of 1 kV. Energy dispersive X-ray analysis (EDX) was performed using an Oxford Instruments X-MAX detector (80 mm^2) at a 20 kV acceleration voltage. Before the measurements, the samples were coated with ~5 nm conductive carbon layer. For the specific surface area measurements, we used a Katakon ATX-06 low-temperature nitrogen adsorption analyzer in a partial pressure range of 0.05–0.25, and the data were processed using a BET model. The skeletal density of the samples was measured with a helium pycnometer, Thermo Fisher Scientific Pycnomatic ATC.

The dielectric properties of pelleted powders were studied using a NOVOCONTROL Alpha-A dielectric relaxometer (Novocontrol Technologies) equipped with an active measuring cell. Measurements were conducted in the frequency range of 10–10^6 Hz, in the temperature range of 223–293 K, in a nitrogen atmosphere at an applied voltage amplitude of 1 V.

To measure the sedimentation stability of the $Bi_{1.8}Fe_{1.2}SbO_7$ suspensions in PMS-300 silicone oil, electrorheological fluids with a concentration of the dispersed phase of 10 wt.% were prepared. For this purpose, $Bi_{1.8}Fe_{1.2}SbO_7$ powder was thoroughly ground in an agate mortar with an aliquot of PMS-300 silicone oil (Penta Silicones) for several hours, until a stable suspension was obtained. To study the stability of colloidal systems, suspensions were placed into 1 or 2 mL plastic syringes. Syringes were set strictly vertical, and special attention was paid to excluding mechanical vibrations and substantial changes in temperature. Sedimentation analysis was performed by determining the position of the boundary of clear liquor in the upper zone of the samples using a cathetometer. The accuracy of the boundary determination was not less than ± 1 mm, at a total height of liquid of 50 mm.

Measurements of the shear stress of electrorheological fluids as a function of field strength and shear rate were conducted using a modified rotational RN-211 CR rheometer with a controlled shear rate and a measurement cell comprising parallel polished brass electrodes (diameter of 20 mm and an interelectrode gap of 1 mm). A voltage of up to 5 kV was applied between the upper sliding contact and the lower stationary electrode. The error in the measured torque value did not exceed 5%. Measurements of the tensile and compressive stress of ERFs at different field strengths were conducted using a computer-controlled press with a fine adjustment screw, the movement of the plunger performed using a step motor. The feed rate of a movable electrode was 0.003 mm/s. The readings of a strain gage (sensitivity of 0.001 g) were automatically stored into a computer memory, and had a frequency of 1 s^{-1}. The field strength in the interelectrode gap in tension or compression measurements was calculated as $E = U/h$, where U is the applied voltage and h is the current value in the interelectrode gap. The initial gap value was 1 mm in tension mode, and 2 mm in compression mode.

Dielectric measurements were conducted in a cylindrical capacitor-type cell with polished stainless steel electrodes. The measurements of the frequency dependence of the dielectric constant and dielectric loss tangent were performed using a Solartron SI 1260 Impedance/Gain-Phase analyzer. For the visualization of electrorheological experiments at ×40 magnification, we used a cell comprising copper electrodes with a gap of 1 mm and which was provided with a video camera. All measurements of electrorheological properties were conducted at room temperature.

3. Results and discussion

Previously we have shown that, in the Bi_2O_3–Fe_2O_3–Sb_2O_x system, the phase with a pyrochlore-type structure crystallizes in a wide range of compositions, and an ideal stoichiometric composition of Bi_2FeSbO_7 falls beyond this region [29,30]. For the synthesis, we used a stoichiometry of Bi:Fe:Sb = 1.8:1.2:1.0, which corresponds to the formula $Bi_{1.8}Fe_{1.2}SbO_7$.

Rietveld refinement of the powder X-ray diffraction data (Fig. 1) confirmed that the crystal structure of the synthesized $Bi_{1.8}Fe_{1.2}SbO_7$ material belongs to the pyrochlore structural type ($Fd3m$). The exact composition of the powder was estimated using the concentration dependence for $Bi_{2-x}Fe_{1+x}SbO_7$ solid solutions [30]. The calculated lattice parameter value ($a = 10.460(3)$ Å, $R_{wp} = 1.88$) corresponded to the $Bi_{1.84}Fe_{1.16}SbO_7$ composition. The chemical composition of the sample was also confirmed by EDX. According to SEM measurements, the synthesized powder consisted of uniform spherical aggregates (140–240 nm) of superfine, nearly monodispersed, 20 nm particles (Fig. 2). The specific surface area and pycnometric density of

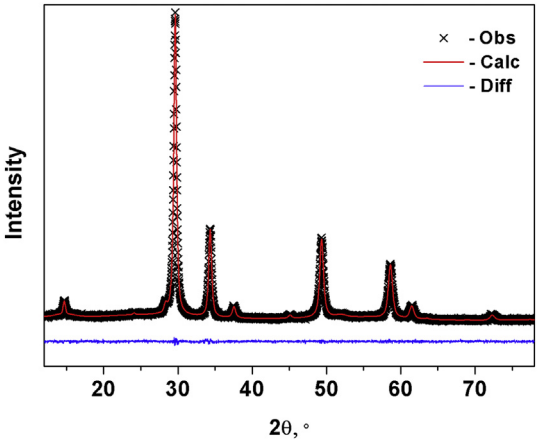

Fig. 1. Experimental (Obs) and calculated (Calc) diffraction patterns of $Bi_{1.8}Fe_{1.2}SbO_7$, and the difference between them (Diff). The diffraction pattern fully coincides with our recently reported data [29].

$Bi_{1.8}Fe_{1.2}SbO_7$ powders was equal to 30 m^2/g and 6.77 g/cm^3, respectively.

Suspensions containing 10 wt.% of $Bi_{1.8}Fe_{1.2}SbO_7$ in PMS-300 silicone oil demonstrated low sedimentation stability due to the high density of the material (Fig. 3). To obtain more stable suspensions we decided to increase the concentration of the dispersed phase, so in further experiments 40.0, 60.0, 80.0 and 90.0 wt.% suspensions were used (0.088, 0.178, 0.366 and 0.461 vol fraction, respectively). The increase in sedimentation stability for concentrated suspensions is due to the strong interparticle interaction that increase the viscosity and reduce the sedimentation rate [31,32]. The suspension containing 90 wt.% of $Bi_{1.8}Fe_{1.2}SbO_7$ in PMS-300 had a very high viscosity, and upon its loading into a cell, air bubbles appeared which hindered dielectric measurements.

The analysis of dielectric spectra (Fig. 4) showed that the relaxation processes in $Bi_{1.8}Fe_{1.2}SbO_7$ suspensions in PMS-300 silicone oil were not of the Debye nature. The dispersion of dielectric permittivity and dielectric loss tangent of the suspensions depended on the concentration of the dispersed phase (Fig. 4), due to the formation of percolation structures consisting of the dispersed phase particles. The increase in the dispersed phase concentration shifted the position of the dielectric loss tangent maximum towards lower frequencies. This effect was accompanied by a sharp increase in dielectric permittivity in the low frequency region. The frequency dependences of dielectric permittivity for suspensions of $Bi_{1.8}Fe_{1.2}SbO_7$ powders were fitted to the Havriliak–Negami equation [33]: $\varepsilon^* = \varepsilon_\infty + \Delta\varepsilon/(1 + (i\omega\tau)^\alpha)^\beta$, where $\Delta\varepsilon = \varepsilon_0 - \varepsilon_\infty$, ε^* is the dielectric permittivity at the circular frequency ω, ε_0 is the dielectric permittivity of the suspension at the zero frequency, ε_∞ is the dielectric permittivity of the suspension at an infinite frequency, and α and β are parameters related to the distribution of relaxation times.

Table 1 summarizes the results of the fitting of the experimental data to the Havriliak–Negami equation. The relaxation times' distribution becomes increasingly asymmetrical, with a shift towards lower frequencies and with an increase in the dispersed filler concentration (Fig. 4a). According to the principle formulated by Hao [34,35], the electrorheological effect should increase as dielectric relaxation time and dielectric loss tangent values increase.

The calculated values of ε_0 and ε_∞ (Table 1) allowed an estimation of the dielectric permittivity of $Bi_{1.8}Fe_{1.2}SbO_7$ at zero and infinite frequencies using the Lichtenecker equation [36],

$$\ln\varepsilon = \Theta_f \cdot \ln\varepsilon_f + \Theta_S \cdot \ln\varepsilon_S$$

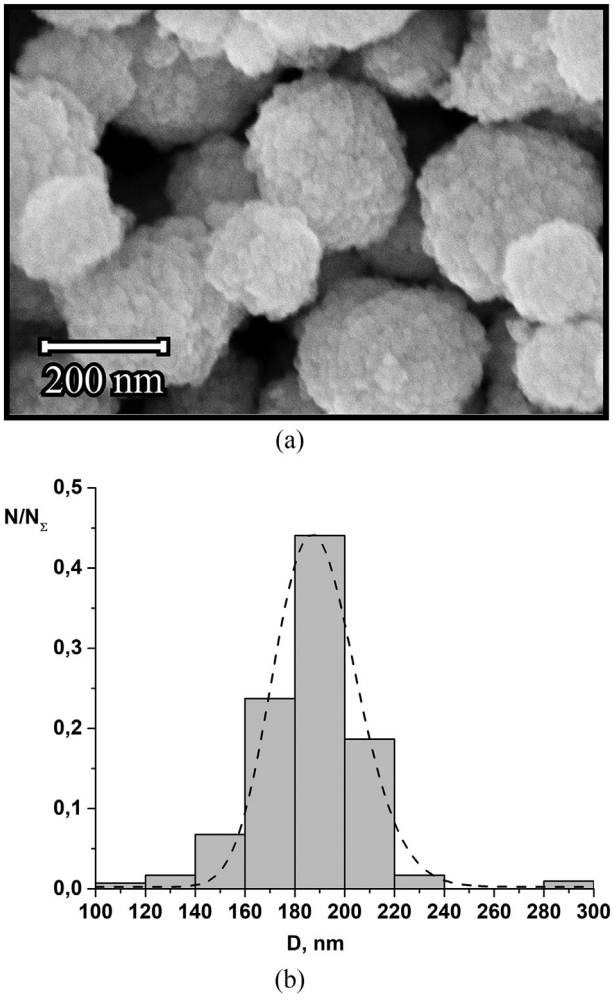

Fig. 2. A typical SEM image of $Bi_{1.8}Fe_{1.2}SbO_7$ powder (a) and particle size distribution derived from SEM data and fitted to a lognormal function (b).

(here, ε is the dielectric permittivity at zero or infinite frequency, Θ_f and Θ_S are the volume fractions of the dispersion medium and the dispersed phase, respectively, and ε_f and ε_S are the dielectric permittivity of the dispersion medium and the dispersed phase, respectively). In our calculations, we used the fact that the ε_f value does not depend on frequency in the 25–10^6 Hz range [37].

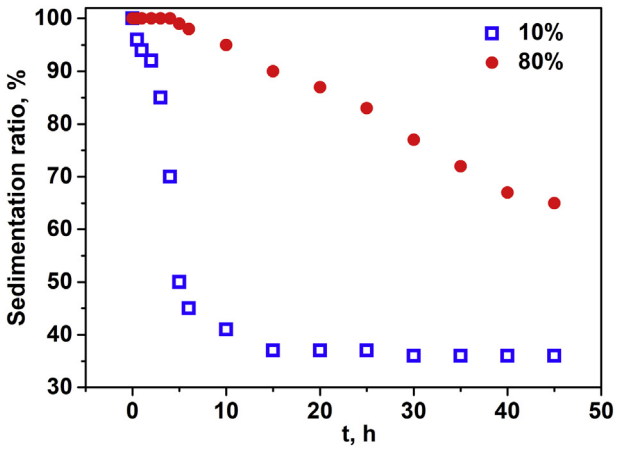

Fig. 3. Sedimentation curves for the suspensions of $Bi_{1.8}Fe_{1.2}SbO_7$ particles (10 or 80 wt.%) in PMS-300 silicone oil. Sedimentation ratio = $(V_{suspension} - V_{sediment})/V_{suspension}$.

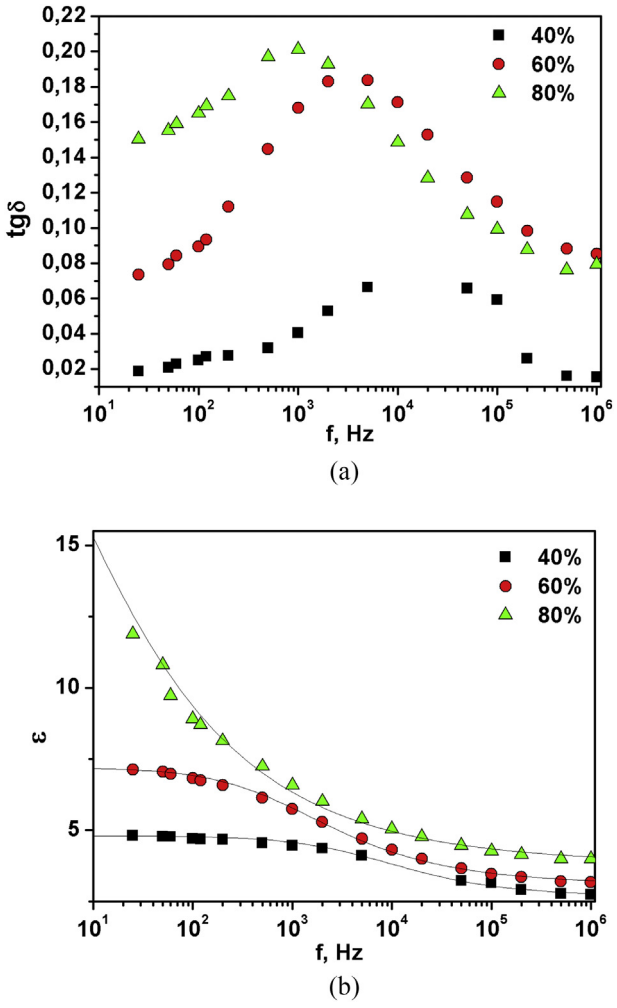

Fig. 4. Dielectric loss tangent (a) and permittivity (b) of $Bi_{1.8}Fe_{1.2}SbO_7$ suspensions of various concentrations (40 wt.%, 60 wt.%, 80 wt.%) in silicone oil as a function of electromagnetic frequency.

The average ε_S values for $Bi_{1.8}Fe_{1.2}SbO_7$ at infinite and zero frequencies were 9.2 ± 0.8 and 1240 ± 150. A considerable decrease in ε_S value upon an increase in frequency (by a factor of more than 100) can be explained by taking into account the significant contribution of conductivity to the value of dielectric permittivity. A similar effect was also observed for bismuth ferrites [38–40].

The observed dielectric relaxation behaviour in $Bi_{1.8}Fe_{1.2}SbO_7$-based ERFs cannot be reliably attributed to dipole or Maxwell-Wagner polarization types, due to the similarity of the corresponding equations. At the same time, the values of relaxation times (ranging from 0.0003 to 0.35 s) favours the interfacial polarization mechanism.

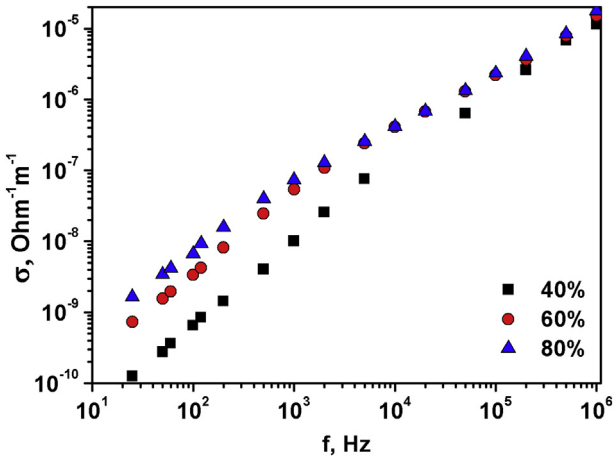

Fig. 5. Frequency dependence of the conductivity of $Bi_{1.8}Fe_{1.2}SbO_7$ based ERFs with various concentrations of the filler (40 wt.%, 60 wt.%, 80 wt.%).

To analyze the contribution of the ERFs' conductivity to the polarization processes, we used a well-known relationship $\sigma_{ac} = \omega \cdot \varepsilon_0 \cdot \varepsilon' \cdot \tan\delta$. Fig. 5 shows that the conductivity of the suspensions at low frequencies increased in the following order: $\sigma_{40\%} < \sigma_{60\%} < \sigma_{80\%}$. Thus, the polarization of $Bi_{1.8}Fe_{1.2}SbO_7$ particles in a constant electric field should increase at high concentrations of the filler.

Fig. 6 shows the results of uniaxial tension measurements of the ERFs at various filler concentrations and electric field strengths. These data show that the increase in dispersed phase concentration resulted in higher yield strength values (the maximum in tensile stress curves). At a field intensity of 5 kV/mm, the yield strengths were 1.38, 2.97, 10.95 and 16.80 kPa for $Bi_{1.8}Fe_{1.2}SbO_7$ concentrations of 40, 60, 80 and 90 wt.%. The maximum in the stress-strain curves for the ERFs containing 40, 60 and 80 wt.% of the filler insignificantly shifted from $(L - L_0)/L_0 \approx 0.3$ at $E = 1$ kV/mm to $(L - L_0)/L_0 \approx 0.5$ at $E = 5$ kV/mm, where L_0 is the starting value of the interelectrode space equal to the fluid layer thickness, L is the current value of the fluid layer thickness under tension or compression. The stress-strain curves for a fluid containing 90 wt.% of the filler had broader peaks (Fig. 6d). For this ERF, the maximum in the stress-strain curve shifted from ~0.5 to ~0.75 upon an increase in the electric field strength.

Young's moduli of the ERFs were calculated as the averaged values for the slopes of the initial sections in the stress-strain curves (Fig. 6): 13.9 kPa (40 wt.%), 41.7 kPa (60 wt.%), 66.5 kPa (80 wt.%) and 72.0 kPa (90 wt.%). Thus, Young's modulus was higher for the ERFs with a higher content of the filler. An increase in the filler content from 80 to 90 wt.% resulted in an increase in the plasticity of the ESR fluid. As a result, the maximum on the stress-strain curve shifted towards higher values of relative stretching. Note that Young's modulus for more concentrated ERFs increased with $\Delta\varepsilon$, dielectric relaxation time (Table 1) and the conductivity of suspensions at low frequencies (Fig. 5).

Table 1
Parameters of the Havriliak–Negami equation for frequency dependences of the dielectric permittivity of $Bi_{1.8}Fe_{1.2}SbO_7$ suspensions in PMS-300 silicone oil with various concentrations of the filler.

Filler concentration, wt.%	ε_∞	ε_0	$\Delta\varepsilon$	α	β	t (s)	Young's modulus (kPa) in an electric field
40%	2.68	4.2	1.52	0.93	0.65	0.00031	13.8
60%	3.10	7.20	4.10	0.95	0.50	0.0019	41.7
80%	3.85	23.20	19.30	1	0.35	0.35	66.5

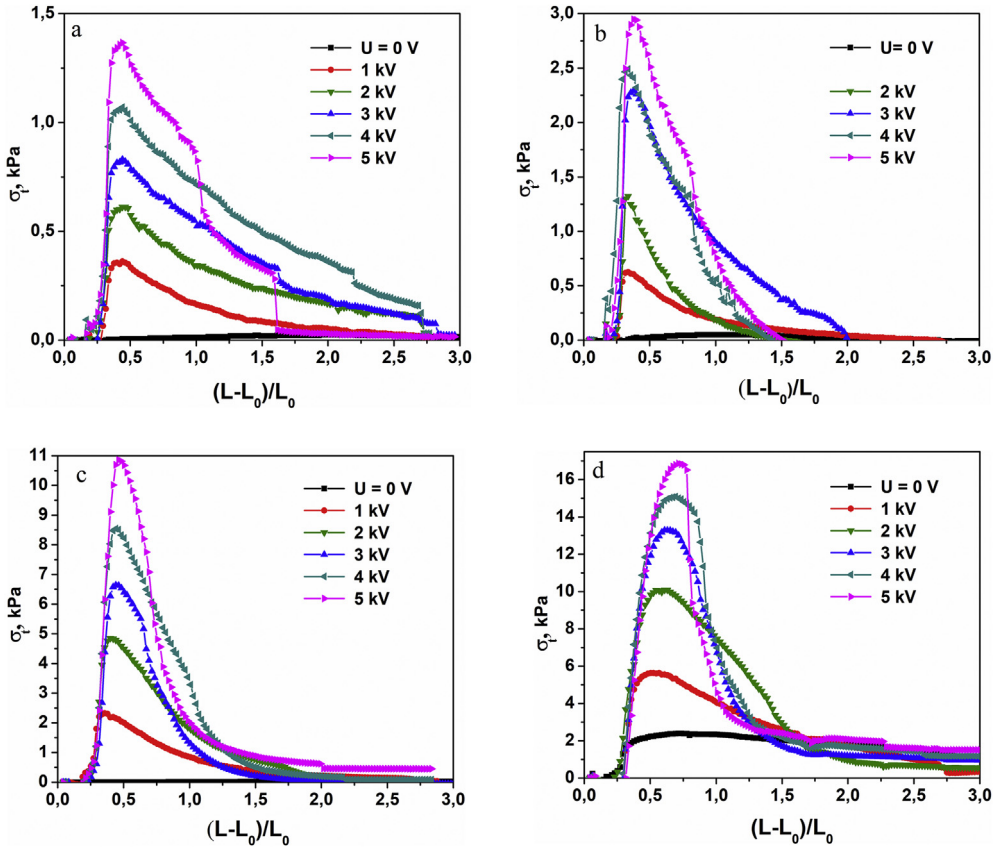

Fig. 6. Tensile stress curves of $Bi_{1.8}Fe_{1.2}SbO_7$ based ERFs containing various concentrations of the filler (a – 40 wt.%, b – 60 wt.%, c – 80 wt.%, d – 90 wt.%). The electric field strengths are indicated in legends. σ_t is the tensile stress.

Fig. 7 shows the results of the compression experiments at various initial electric field strengths for ERFs with various concentrations of $Bi_{1.8}Fe_{1.2}SbO_7$. The values of compressive strength continuously increased with a change in compression ratio, due to two factors. First, the field strength in the interelectrode gap continuously increased as the electrodes came closer together. Second, in an applied electric field, the particles of the filler formed relatively rigid chain-like structures, and upon the compression of the structured ERF the silicone oil squeezed out of the suspension resulting in an increase in the concentration of the filler. Fig. 7 shows that the compressive strength of the ERF in an electric field, $P = F/S$ (here, F is the force that is applied to the piston having an area S), demonstrated an almost linear behaviour for 40 and 60 wt.% filler suspensions and a nearly parabolic behaviour for filler suspensions of 80 and 90 wt.%.

At the same time, the compression of an electrorheological fluid can be represented as a transformed shear flow [41]. When the fluid is compressed in a cell between two parallel electrodes at a very low rate, the effect of viscous forces can be discounted. In this case, the compressive strength of an electrorheological fluid in an electric field can be expressed in terms of the shear stress (τ), and the geometry of the cell [42] $P = \frac{D}{3h}\tau_0$, whence it follows that $\tau_0 = \frac{P \cdot 3h}{D}$.

The compressive shear stress curves for ERFs with various concentrations of $Bi_{1.8}Fe_{1.2}SbO_7$ (Fig. 8) illustrate an almost similar saturation behaviour. The curves contain the region corresponding to viscoelastic compression, a transition region and the region close to saturation. Each region corresponds to the following regimes:

1. viscoelastic compression is due to the compaction of the structures formed by the dispersed particles, the strengthening of the bonds between the polarized molecules of the dispersion medium and filler particles, and the formation and strengthening of the bridging structures in the fluid;
2. the transition region is associated with the beginning of the destruction of the structures in the fluid and the squeezing of the liquid from the interelectrode gap;
3. squeezing of the electrorheological fluid from the interelectrode gap.

The length of each region and τ_0 value depend on the $Bi_{1.8}Fe_{1.2}SbO_7$ concentration and the electric field strength. Thus, the compression mechanism of the ERFs based on $Bi_{1.8}Fe_{1.2}SbO_7$ most probably does not depend on the concentration of the filler.

The inflection points in the $\tau \sim (L_0 - L)/L_0$ curves shift towards higher field strengths at a fixed concentration of the filler, and towards higher strains upon the increase in the concentration of the filler.

The electric field strength dependencies of shear viscosity and shear stress at 16 s^{-1} shear rate for the ERFs with various filler concentrations (Fig. 9) demonstrated classic behaviour. Up to certain electric field strength values, the changes in shear viscosity and shear stress values were insignificant, while with stronger electric fields ERFs exhibited an increase in shear resistance. At a low filler concentration (40 wt.%), the threshold electric field strength was about 2 kV/mm, while with higher filler content it was 1 kV/mm. Such a threshold-related electrorheological effect is typical for systems demonstrating the polarization mechanism of particle interaction [1–4].

We compared the efficiency of the electrical energy conversion into mechanical energy for the ERFs containing various concentrations of the filler according to previously reported recommendations [43,44]. For this purpose, the relative viscosities of ERFs

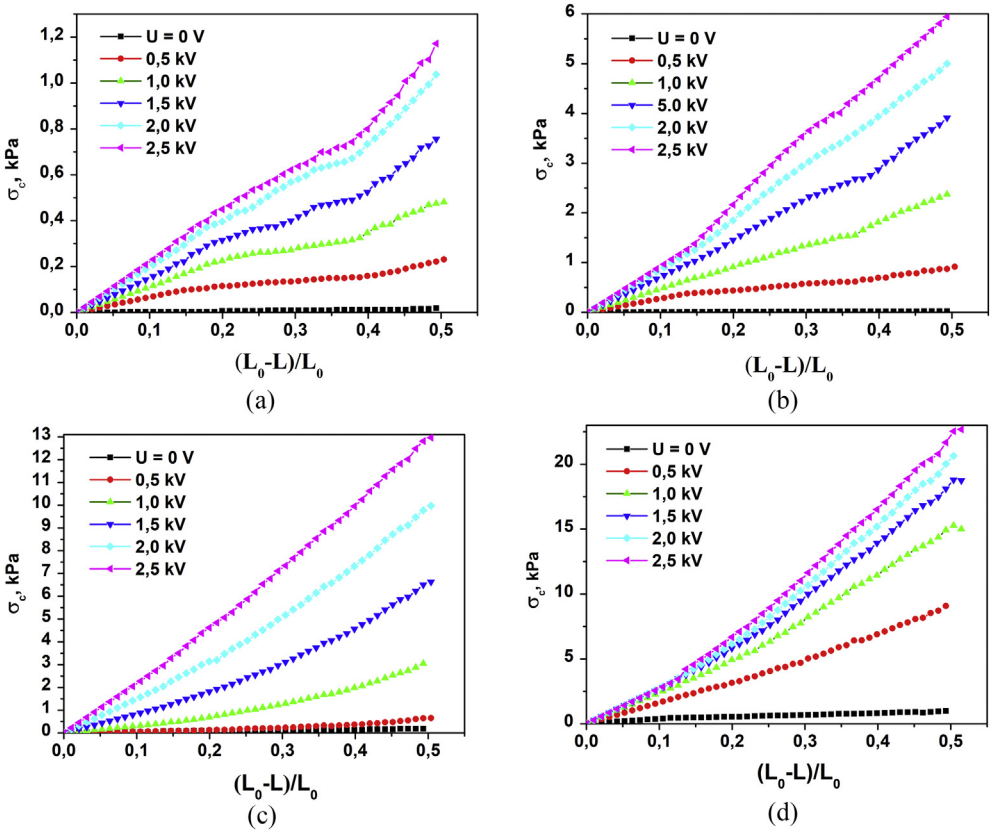

Fig. 7. Compressive strength curves of $Bi_{1.8}Fe_{1.2}SbO_7$ based ERFs containing various concentrations of the filler (a – 40 wt.%, b – 60 wt.%, c – 80 wt.%, d – 90 wt.%). The electric field strengths are indicated in legends. σ_c is the compressive stress.

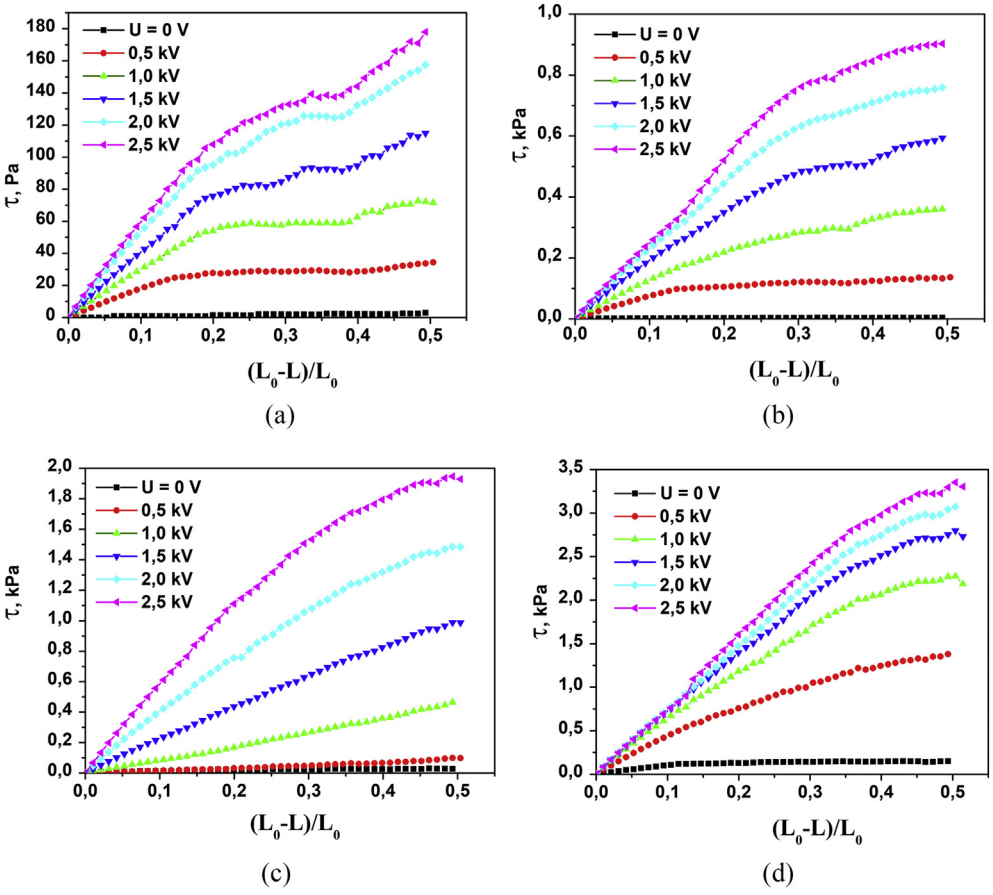

Fig. 8. Compressive shear stress curves of $Bi_{1.8}Fe_{1.2}SbO_7$ based ERFs containing various concentrations of the filler (a - 40 wt.%, b - 60 wt.%, c - 80 wt.%, d - 90 wt.%) for various electric field strengths.

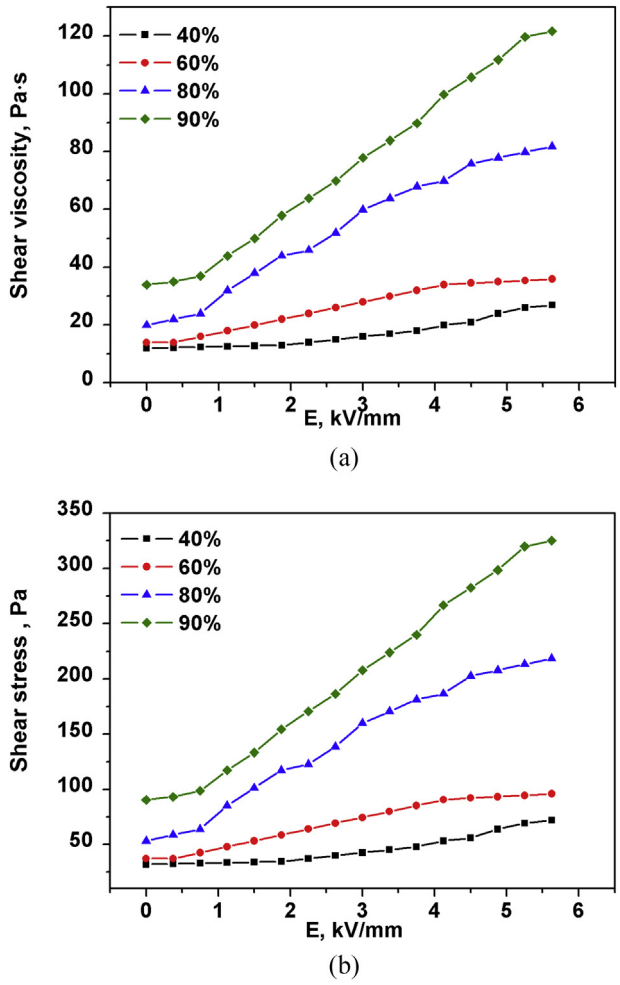

Fig. 9. Shear viscosity (a) and tangential shear stress (b) at various electric field strengths for $Bi_{1.8}Fe_{1.2}SbO_7$ based ERFs containing various concentrations of the filler at a shear rate of 16 s^{-1}.

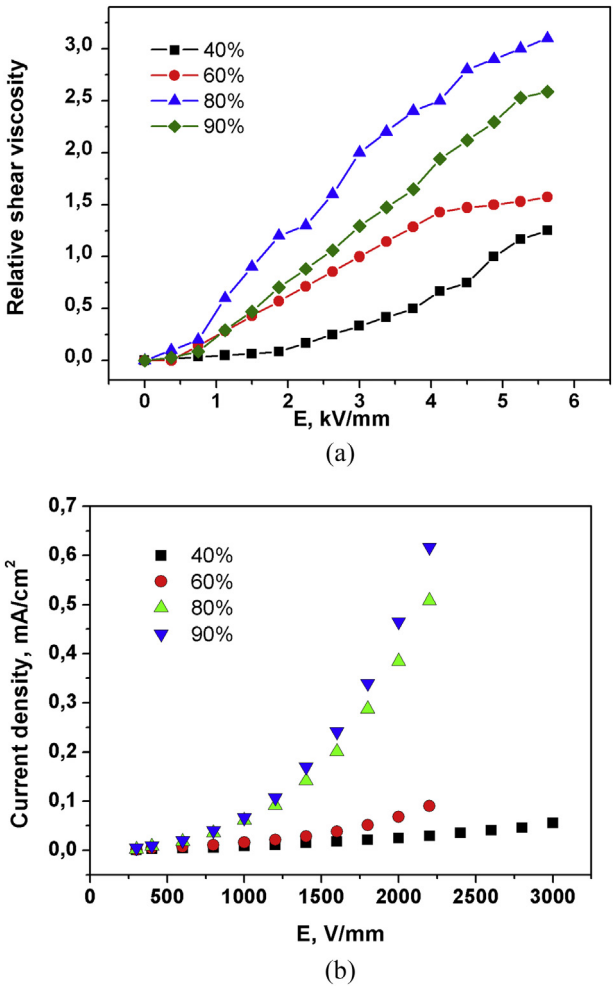

Fig. 10. (a) Electrorheological efficiency for ERFs with various filler concentrations; (b) the electric current density *vs* electric field strength for ERFs with various filler concentrations, an interelectrode gap was 1 mm.

were plotted against the electric field strength (Fig. 10a). Our data showed that the highest efficiency was reached for the ERF containing 80 wt.% of the filler. Most likely, lower efficiencies for 40 and 60 wt.% suspensions were due to the loose interparticle contacts, while 80 and 90 wt.% suspensions reached the percolation threshold allowing for strong contacts between the filler particles. On the other hand, liquid-depleted strong contacts between the particles in 90 wt.% suspension resulted in a high yield strength and high viscosity of the corresponding ERF and reduced its electrorheological efficiency.

The formation of strong interparticle contacts in highly concentrated (80 and 90 wt.%) suspensions was corroborated by the density of the electric current flowing through the interelectrode gap measured at various electric field strengths and filler concentrations (Fig. 10b).

The data presented in Fig. 10 can also be discussed in terms of the mechanism of suspensions' behaviour in an electric field [45]. Highly non-linear dependence of the relative viscosity *vs* electric field strength for the ERF containing 40 wt.% of the filler indicates that the increase in the electric field strength results in significant changes in both the distances between the particles and their polarization. On the other hand, almost linear dependencies for the highly concentrated suspensions indicated that the dense interparticle contacts inherent to these systems prevented the changes in interparticle distances upon the application of the electric field. At this point, the polarizability of the particles in the liquid remained constant and electrorheological effect varied proportionally to the applied electric field.

4. Conclusions

Superfine powders of pure $Bi_{1.8}Fe_{1.2}SbO_7$, with a pyrochlore structure and containing hierarchically organized ~200 nm spherical particles, were synthesized *via* the microwave-hydrothermal method. The dielectric characteristics of the suspensions of $Bi_{1.8}Fe_{1.2}SbO_7$ in PMS-300 silicone oil, (dielectric permittivity, dielectric loss tangent and conductivity), as a function of $Bi_{1.8}Fe_{1.2}SbO_7$ concentration in the frequency range of 25–10^6 Hz, were studied. The values of the dielectric permittivity of $Bi_{1.8}Fe_{1.2}SbO_7$ superfine powders at zero and infinite frequencies were calculated using the Lichtenecker equation. The electrorheological effect in the $Bi_{1.8}Fe_{1.2}SbO_7$ suspensions under an applied electric field with strengths up to 5 kV/mm was studied for the first time in tensile stress, compressive strength and shear stress modes. The high value of the electrorheological effect (yield strength of ~20 kPa at 5 kV/mm) was due to the considerable contribution of conductivity to polarization.

Acknowledgments

This study was financially supported by the Russian Science Foundation (project no. 16-13-10399). This research was performed using the equipment of the JRC PMR IGIC RAS.

Appendix A. Supplementary data

Supplementary data to this article can be found online at https://doi.org/10.1016/j.powtec.2019.10.027.

References

[1] A.V. Agafonov, A.G. Zakharov, Electrorheological fluids, Russ. J. Gen. Chem. 80 (2010) 567–575, https://doi.org/10.1134/S1070363210030382.
[2] W.M. Winslow, Induced fibration of suspensions, J. Appl. Phys. 20 (1949) 1137–1140, https://doi.org/10.1063/1.1698285.
[3] L. Marshall, C.F. Zukoski, J.W. Goodwin, Effects of electric fields on the rheology of non-aqueous concentrated suspensions, J. Chem. Soc., Faraday Trans. 1 (85) (1989) 2785–2795, https://doi.org/10.1039/F19898502785.
[4] A.V. Lykov, Z.P. Shulman, Yu.F. Deynega, Elektroreologicheskiy Effect, Nauka i tekhnika, Minsk, 1972 , (in Russ.).
[5] D.M. Heyes, J.R. Melrose, Brownian dynamics simulations of electro-rheological fluids, II, Mol. Simul. 5 (1990) 293–306, https://doi.org/10.1080/08927029008022415.
[6] A.A. Mokejev, E.V. Korobko, L.G. Vedernikova, Structural viscosity of electrorheological fluids, J. Non-Newtonian Fluid Mech. 42 (1992) 213–230, https://doi.org/10.1016/0377-0257(92)80010-U.
[7] R.T. Bonnecaze, J.F. Brady, Dynamic simulation of an electrorheological fluid, J. Chem. Phys. 96 (1992) 2183–2202, https://doi.org/10.1063/1.462070.
[8] J.E. Martin, R.A. Anderson, Chain model of electrorheology, J. Chem. Phys. 104 (1996) 4814–4827, https://doi.org/10.1063/1.471176.
[9] R. Tao, Q. Jiang, Simulation of structure formation in an electrorheological fluid, Phys. Rev. Lett. 73 (1994) 205–208, https://doi.org/10.1103/PhysRevLett.73.205.
[10] Yu.G. Yanovskii, V.E. Zgaevskii, Yu.N. Karnet, I.F. Obraztsov, Electrorheological fluids. Theoretical and experimental approaches to their description, Phys. Mesomech. 6 (2003) 61–69.
[11] J. Lu, X. Zhao, Electrorheological properties of suspensions based on polyaniline-montmorillonite clay nanocomposite, J. Mater. Res. 17 (2002) 1513–1519, https://doi.org/10.1557/JMR.2002.0225.
[12] S.G. Kim, J.W. Kim, W.H. Jang, H.J. Choi, M.S. Jhon, Electrorheological characteristics of phosphate cellulose-based suspensions, Polymer 42 (2001) 5005–5012, https://doi.org/10.1016/S0032-3861(00)00887-9.
[13] T. Plachy, M. Masar, M. Mrlik, M. Machovsky, Z. Machovska, E. Kutalkova, I. Kuritka, Switching between negative and positive electrorheological effect of g-C_3N_4 by copper ions doping, Adv. Powder Technol. 30 (2019) 714–723, https://doi.org/10.1016/j.apt.2019.01.001.
[14] X.P. Zhao, X. Duan, In sol-gel preparation of polysaccharide/titanium oxide hybrid colloids and their electrorheological effect, J. Colloid Interface Sci. 251 (2002) 376–380, https://doi.org/10.1006/jcis.2002.8281.
[15] A.V. Agafonov, A.S. Krayev, O.I. Davydova, K.V. Ivanov, T.O. Shekunova, A.E. Baranchikov, O.S. Ivanova, L.P. Borilo, A.V. Garshev, V.V. Kozik, V.K. Ivanov, Nanocrystalline ceria: a novel material for electrorheological fluids, RSC Adv. 6 (2016) 88851–88858, https://doi.org/10.1039/C6RA15095K.
[16] Y.D. Liu, F.F. Fang, H.J. Choi, Y. Seo, Fabrication of semiconducting polyaniline/nanosilica nanocomposite particles and their enhanced electrorheological and dielectric characteristics, Colloid. Surf. Physicochem. Eng. Asp. 381 (2011) 17–22, https://doi.org/10.1016/j.colsurfa.2011.02.051.
[17] Y. Liu, R.L. Withers, H. Chen, Q. Li, H. Tan, Raman spectra, photoluminescence and dielectric relaxation in $Bi_{1.5}ZnNb_{1.5}O_7$ pyrochlore, Curr. Appl. Phys. 11 (2011) S171–S174, https://doi.org/10.1016/j.cap.2011.03.014.
[18] S.W. Jiang, Y.R. Li, R.G. Li, N.D. Xiong, L.F. Tan, X.Z. Liu, B.W. Tao, Dielectric properties and tunability of cubic pyrochlore $Bi_{1.5}MgNb_{1.5}O_7$ thin films, Appl. Phys. Lett. 94 (2009) 162908-1–162908-3, https://doi.org/10.1063/1.3126442.
[19] L.X. Li, X.Y. Zhang, L.J. Ji, P.F. Ning, Q.W. Liao, Dielectric properties and electrical behaviors of tunable $Bi_{1.5}MgNb_{1.5}O_7$ thin films, Ceram. Int. l38 (2012) 3541–3545, https://doi.org/10.1016/j.ceramint.2011.12.069.
[20] J. Lu, S. Stemmer, Low-loss, tunable bismuth zinc niobate films deposited by rf magnetron sputtering, Appl. Phys. Lett. 83 (2003) 2411–2413, https://doi.org/10.1063/1.1613036.
[21] J.Y. Kim, D.W. Kim, H.S. Jung, K.S. Hong, Voltage-tunable dielectric properties of pyrochlore Bi–Zn–Nb–Ti–O solid-solution thin films, Jpn. J. Appl. Phys. 44 (2005) 6648–6653, https://doi.org/10.1143/JJAP.44.6648.
[22] Y. Liu, R.L. Withers, H.B. Nguyen, K. Elliott, Q. Ren, Z. Chen, Displacive disorder and dielectric relaxation in the stoichiometric bismuth-containing pyrochlores $Bi_2M^{III}NbO_7$ (M=In and Sc), J. Solid State Chem. 182 (2009) 2748–2755, https://doi.org/10.1016/j.jssc.2009.07.007.
[23] D. Huiling, Y. Xi, Structural trends and dielectric properties of Bi-based pyrochlores, J. Mater. Sci. Mater. Electron. 15 (2004) 613–616, https://doi.org/10.1023/B:JMSE.0000036041.84889.b2.
[24] H. Wang, H. Du, Z. Peng, M. Zhang, X. Yao, Improvements of sintering and dielectric properties on Bi_2O_3–ZnO–Nb_2O_5 pyrochlore ceramics by V_2O_5 substitution, Ceram. Int. 30 (2004) 1225–1229, https://doi.org/10.1016/j.ceramint.2003.12.076.
[25] W. Somphon, V. Ting, Y. Liu, R.L. Withers, Q. Zhou, B.J. Kennedy, Local crystal chemistry, structured diffuse scattering and the dielectric properties of $(Bi_{1-x}Y_x)_2(M^{III}Nb^{V})O_7$ (M = Fe^{3+}, In^{3+}) Bi-pyrochlores, J. Solid State Chem. 179 (2006) 2495–2505, https://doi.org/10.1016/j.jssc.2006.04.046.
[26] M.P. Chon, K.B. Tan, C.C. Khaw, Z. Zainal, Y.H. Taufiq-Yap, P.Y. Tan, Synthesis, structural and electrical properties of novel pyrochlores in the Bi_2O_3–CuO–Ta_2O_5 ternary system, Ceram. Int. 38 (2012) 4253–4261, https://doi.org/10.1016/j.ceramint.2012.02.007.
[27] M. Valant, G.S. Babu, M. Vrcon, T. Kolodiazhnyi, A.-K. Axelsson, Pyrochlore range from Bi_2O_3–Fe_2O_3–TeO_3 system for LTCC and photocatalysis and the crystal structure of new $Bi_3(Fe_{0.56}Te_{0.44})_3O_{11}$, J. Am. Ceram. Soc. 95 (2012) 644–650, https://doi.org/10.1111/j.1551-2916.2011.04801.x.
[28] A.V. Egorysheva, O.M. Gajtko, P.O. Rudnev, O.G. Ellert, Vladimir K. Ivanov, Synthesis of Bi-Fe-Sb-O pyrochlore nanoparticles with the visible-light photocatalytic activity, Eur. J. Inorg. Chem. 2016 (2016) 2193–2199, https://doi.org/10.1002/ejic.201501159.
[29] A.V. Egorysheva, O.G. Ellert, Yu.V. Maksimov, V.D. Volodin, N.N. Efimov, V.M. Novotortsev, Subsolidus phase equilibria and magnetic characterization of the pyrochlore in the Bi_2O_3-Fe_2O_3-Sb_2O_x system, J. Alloy. Comp. 579 (2013) 311–314, https://doi.org/10.1016/j.jallcom.2013.06.096.
[30] A.V. Egorysheva, O.G. Ellert, O.M. Gajtko, N.N. Efimov, R.D. Svetogorov, Y.V. Zubavichus, A.V. Grigorieva, The Bi_2O_3-Fe_2O_3-Sb_2O_5 system phase diagram refinement, $Bi_3FeSb_2O_{11}$ structure peculiarities and magnetic properties, J. Solid State Chem. 225 (2015) 278–284, https://doi.org/10.1016/j.jssc.2014.12.032.
[31] J.I. Bhatty, K.J. Reid, D. Dollimore, T.H. Shah, G.A. Gamlen, A. Tamimi, Suspensions and sediments. Part II. Behavior of concentrated suspensions, Separ. Sci. Technol. 24 (1989) 165–178, https://doi.org/10.1080/01496398908049761.
[32] H. Kourki, M.H.N. Famili, Particle sedimentation: effect of polymer concentration on particle–particle interaction, Powder Technol. 221 (2012) 137–143, https://doi.org/10.1016/j.powtec.2011.12.050.
[33] S. Havriliak, S. Negami, A complex plane representation of dielectric and mechanical relaxation processes in some polymers, Polymer 8 (1967) 161–210, https://doi.org/10.1016/0032-3861(67)90021-3.
[34] T. Hao, Z. Xu, Y. Xu, Correlation of the dielectric properties of dispersed particles with the electrorheological effect, J. Colloid Interface Sci. 190 (1997) 334–340, https://doi.org/10.1006/jcis.1997.4871.
[35] T. Hao, Electrorheological suspensions, Adv. Colloid Interface Sci. 97 (2002) 1–35, https://doi.org/10.1016/S0001-8686(01)00045-8.
[36] K. Lichtenecker, K. Rother, Die herleitung des logarithmischen Mischungs-gesetzen aus allgemeinen Prinzipien der stationaren Stromung, Physik. Zeithschr. 32 (1931) 255–260.
[37] A.V. Agafonov, O.I. Davydova, A.S. Krayev, O.S. Ivanova, O.L. Evdokimova, T.V. Gerasimova, A.E. Baranchikov, V.V. Kozik, V.K. Ivanov, Unexpected effects of activator molecules' polarity on the electroreological activity of titanium dioxide nanopowders, J. Phys. Chem. B 121 (2017) 6732–6738, https://doi.org/10.1021/acs.jpcb.7b04131.
[38] G.S. Arya, R.K. Kotnala, N.S. Negi, Structural and multiferroic properties of $Bi_{1-x}In_xFeO_3$ (0≤x≤0.20) nanoparticles, J. Appl. Phys. 113 (2013), 044107. https://doi.org/10.1063/1.4788668.
[39] M.R. Biswal, J. Nanda, N.C. Mishra, S. Anwar, A. Mishra, Dielectric and impedance spectroscopic studies of multiferroic $BiFe_{1-x}Ni_xO_3$, Adv. Mat. Lett. 5 (2014) 531–537, https://doi.org/10.5185/amlett.2014.4566.
[40] M. Rangia, S. Sanghia, S. Jangra, K. Kaswana, S. Khasa, A. Agarwa, Crystal structure transformation and improved dielectric and magnetic properties of La-substituted $BiFeO_3$ multiferroics, Ceram. Int. 43 (2017) 12095–12101, https://doi.org/10.1016/j.ceramint.2017.06.065.
[41] Y. Tian, K.Q. Zhu, Y.G. Meng, S.Z. Wen, Mechanical properties of electrorheological fluids, Int. J. Mod. Phys. B 19 (2005) 1311–1317, https://doi.org/10.1142/S0217979205030232.
[42] D.K. Gartling, N. Phan-Thien, A numerical simulation of a plastic fluids in a parallel-plate plastometer, J. Non-Newtonian Fluid Mech. 14 (1984) 347–360, https://doi.org/10.1016/0377-0257(84)80053-1.
[43] K. He, Q. Wen, C. Wang, B. Wang, S. Yu, C. Hao, K. Chen, A facile synthesis of hierarchical flower-like TiO_2 wrapped with MoS_2 sheets nanostructure for enhanced electrorheological activity, Chem. Eng. J. 349 (2018) 416–427, https://doi.org/10.1016/j.cej.2018.05.102.
[44] Z. Wang, X. Song, B. Wang, X. Tian, C. Hao, K. Chen, Bionic cactus-like titanium oxide microspheres and its smart electrorheological activity, Chem. Eng. J. 256 (2014) 268–279, https://doi.org/10.1016/j.cej.2014.06.115.
[45] A.V. Agafonov, A.S. Kraev, O.S. Ivanova, O.L. Evdokimova, T.V. Gerasimova, A.E. Baranchikov, V.V. Kozik, V.K. Ivanov, Comparative study of the electrorheological effect in suspensions of needle-like and isotropic cerium dioxide nanoparticles, Rheol. Acta 57 (2018) 307–315, https://doi.org/10.1007/s00397-018-1076-x.